Trifunctional lipid probes for comprehensive studies of single lipid species in living cells

Doris Höglinger[a,b], André Nadler[a,c], Per Haberkant[a], Joanna Kirkpatrick[a,d], Martina Schifferer[a], Frank Stein[a], Sebastian Hauke[a], Forbes D. Porter[e], and Carsten Schultz[a,1]

[a]Cell Biology and Biophysics Unit, European Molecular Biology Laboratory, 69117 Heidelberg, Germany; [b]Department of Pharmacology, University of Oxford, Oxford OX1 3QT, United Kingdom; [c]Max Planck Institute of Molecular Cell Biology and Genetics, 01307 Dresden, Germany; [d]Leibniz Institute on Aging – Fritz Lipmann Institute, 07745 Jena, Germany; and [e]Division of Translational Medicine, Eunice Kennedy Shriver National Institute of Child Health and Human Development, National Institutes of Health, Bethesda, MD 20892

Edited by Steven G. Boxer, Stanford University, Stanford, CA, and approved December 23, 2016 (received for review July 7, 2016)

Lipid-mediated signaling events regulate many cellular processes. Investigations of the complex underlying mechanisms are difficult because several different methods need to be used under varying conditions. Here we introduce multifunctional lipid derivatives to study lipid metabolism, lipid–protein interactions, and intracellular lipid localization with a single tool per target lipid. The probes are equipped with two photoreactive groups to allow photoliberation (uncaging) and photo–cross-linking in a sequential manner, as well as a click-handle for subsequent functionalization. We demonstrate the versatility of the design for the signaling lipids sphingosine and diacylglycerol; uncaging of the probe for these two species triggered calcium signaling and intracellular protein translocation events, respectively. We performed proteomic screens to map the lipid-interacting proteome for both lipids. Finally, we visualized a sphingosine transport deficiency in patient-derived Niemann–Pick disease type C fibroblasts by fluorescence as well as correlative light and electron microscopy, pointing toward the diagnostic potential of such tools. We envision that this type of probe will become important for analyzing and ultimately understanding lipid signaling events in a comprehensive manner.

lipid–protein interaction | sphingosine | diacylglycerol | caged lipids | Niemann–Pick disease type C

The roles of lipids in cells go far beyond providing the structural backbone of cellular membranes. Certain lipid species are powerful signaling molecules. Examples include the roles of sphingosine (Sph) and the diacylglycerol (DAG) variant, stearoyl-arachidonylglycerol (SAG) in intracellular calcium signaling (1, 2). The study of such signaling lipids is often complicated by the fact that they are under tight metabolic control and that they occur only in very low concentrations. Overexpression of metabolic enzymes for manipulation of signaling lipid levels is a slow process compared with the rapid turnover of those lipids and may therefore produce not only the target lipid but also multiple downstream metabolites. Chemical dimerizer and optogenetic approaches are options to manipulate lipid contents more rapidly, but they depend on cytosolic lipid-metabolizing enzymes. In the past, many applications therefore focused on phosphoinositides (3, 4). A more general way to rapidly increase lipid concentration is the use of caged lipids. These are equipped with a photocleavable protecting group (caging group), which blocks biological activity and renders them resistant to metabolic turnover before the active lipid is released using a flash of light (2, 5–7). The sudden increase in target lipid concentration facilitates analysis of downstream lipid signaling events as well as lipid metabolism within living cells in pulse–chase experiments. To correctly interpret such signaling events, underlying processes such as lipid–protein interactions, intracellular lipid localization, and kinetics of lipid metabolism need to be considered. To date, lipid metabolism is typically monitored using isotope-labeled or alkyne-modified lipids (8–10). Fluorescent lipids, lipid-binding antibodies, or lipid biosensors are mainly used to study lipid localization (11, 12). Most assays for studying lipid–protein interactions rely on reconstituted membranes/liposomes and are therefore largely restricted to soluble proteins (13–16). The plethora of methods used to investigate these different processes makes it difficult to compare or validate their respective results. A promising approach to integrate the study of lipid metabolism, lipid localization, and lipid–protein interactions has emerged in recent years; bifunctional lipids feature a small diazirine group to allow photo–cross-linking with interacting proteins in the intact cellular environment and a terminal alkyne for subsequent functionalization (17). Biotinylation of cross-linked lipid–protein conjugates enables their enrichment and identification of lipid-interacting proteins. To date, bifunctional lipids are one of the few methods to screen for lipid–protein interactions in living cells (18–21). Alternatively, bifunctional lipids can be used to visualize lipid localization by click reaction with a fluorophore (1, 18, 20). The application of the bifunctional lipid principle to signaling lipids, however, is handicapped by their tight metabolic control. Any precursor is rapidly incorporated into downstream lipids, complicating the interpretation of resulting data. The ability to liberate a single, well-defined signaling lipid species within cells and to immediately capture its interacting partners, investigate downstream signaling, and study its subcellular localization would enable much-needed insight into the regulation of lipid-dependent signaling. Here, we present "trifunctional" lipids as tools, combining the advantages of caged and bifunctional lipids in a single molecule to allow for a wide range of studies in living cells with tight temporal control. Applied to Sph and DAG, we show that

Significance

Some lipids such as sphingosine and diacylglycerol are potent signaling effectors. However, comprehensive investigations of their bioactive actions are often hampered by a lack of tools that can be used in living cells. Here, we present chemically modified lipids that allow investigation of acute lipid signaling, lipid metabolism, lipid–protein interactions, and lipid localization by using a single probe for each target lipid. Equipped with a caging group, the lipid probe is biologically inactive, until activated by a flash of light. A second photoreaction cross-links the probe to protein interactors that may subsequently be analyzed by mass spectrometry or fluorescence/electron microscopy. We envision that this versatile design will be central to unraveling complex lipid signaling networks.

Author contributions: D.H., A.N., and C.S. designed research; D.H., A.N., J.K., and M.S. performed research; A.N., P.H., S.H., and F.D.P. contributed new reagents/analytic tools; D.H., A.N., P.H., J.K., M.S., and F.S. analyzed data; and D.H., A.N., F.S., and C.S. wrote the paper.

The authors declare no conflict of interest.

This article is a PNAS Direct Submission.

Freely available online through the PNAS open access option.

[1]To whom correspondence should be addressed. Email: schultz@embl.de.

This article contains supporting information online at www.pnas.org/lookup/suppl/doi:10.1073/pnas.1611096114/-/DCSupplemental.

trifunctional lipids enable (*i*) acute alteration of signaling lipid concentration, (*ii*) measurement of lipid metabolism on a population-wide as well as on a single-cell level, (*iii*) screening for lipid–protein interactions, and (*iv*) direct visualization of lipid localization by light and correlative light and electron microscopy (CLEM) in comparable experimental settings.

Results

Synthesis of Trifunctional Sphingosine, Trifunctional Diacylglycerol, and a Trifunctional Fatty Acid. The previously reported (20) bifunctional sphingosine **4** was equipped with a coumarin caging group via carbamate linkage at the amino group giving the trifunction sphingosine (TFS **1**) in 96% yield (Fig. 1*A*). Synthesis of trifunctional diacylglycerol (TFDAG **2**) started by para-methoxybenzyl (PMB) protection of the free hydroxyl group of *S*-isopropylidene glycerol followed by removal of the isopropylidene group to give diol **6**. Dimethoxytrityl (DMT) protection of the primary hydroxyl group and attachment of arachidonic acid to the secondary hydroxyl group gave intermediate **7**. The PMB-protected diacylglycerol **8** was obtained by mild DMT deprotection using $FeCl_3$ in MeOH/dichloromethane and carbodiimide-mediated coupling of the bifunctional fatty acid **9**. The PMB group was removed by brief exposure to acidic conditions at 0 °C, effectively preventing acyl migration as the only possible alternative regioisomer was not detected by NMR. Lastly, *N*,*N*-diethylaminocoumarin was linked to the primary hydroxyl of **10**, giving the TFDAG **2** (Fig. 1*B*). The trifunctional fatty acid (TFFA **3**) was obtained by standard carbodiimide-mediated attachment of the coumarin group (Fig. 1*C*).

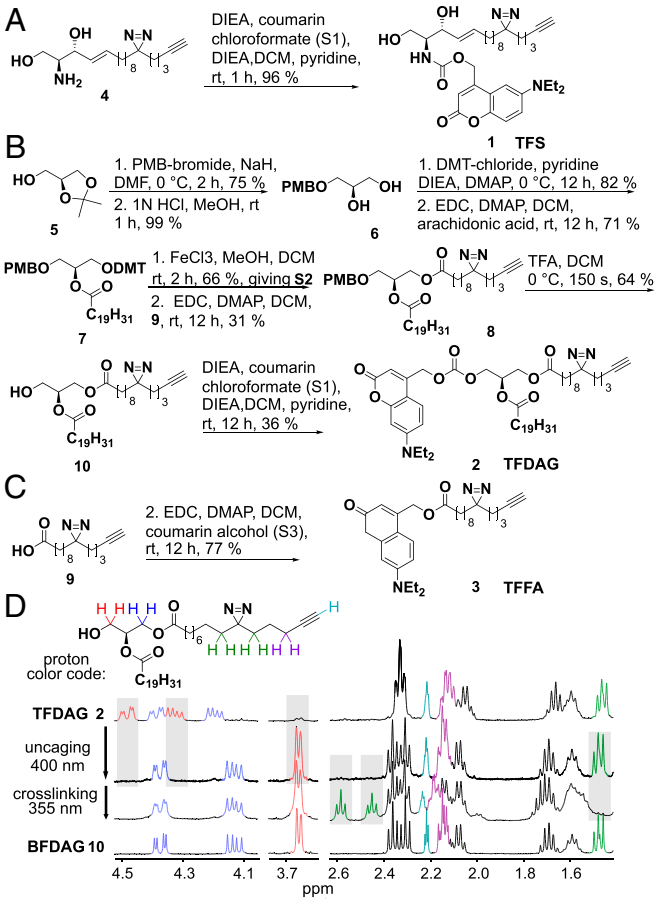

Fig. 1. Synthesis of trifunctional lipids **1** to **3** featuring a photocage, a cross-linkable diaziridine group, and an alkyne. (*A*) Synthesis of trifunctional sphingosine (TFS, **1**). (*B*) Synthesis of trifunctional diacylglycerol (TFDAG, **2**). (*C*) Synthesis trifunctional fatty acid (TFFA, **3**). (*D*) Aliphatic section of the ^{1}H NMR spectrum of the TFDAG. Samples were irradiated for 2 min with >400-nm light and for 2 min with >345-nm light. The latter reaction produces a ketone. A spectrum of bifunctional DAG (BFDAG, **10,** bottom) is shown for comparison.

In Vitro Validation of Sequential Photoreactions. We established that the photoreactions used for uncaging and cross-linking are indeed orthogonal and may be carried out in a sequential manner. To this end, a 1 mM solution of TFDAG **2** in MeOH-d4 was irradiated using a UV mercury arc source equipped with 400-nm and 355-nm high-pass filters. The uncaging reaction was performed at >400 nm, whereas photo–cross-linking the diazirine group required 355-nm light. ^{1}H NMR spectra were acquired after each irradiation step and compared with the spectrum of the corresponding pure compounds **2** and **10** (Fig. 1*D*). We found that uncaging at >400 nm quantitatively removed the coumarin group, as signals stemming from the protons in the glycerol backbone (highlighted in blue and red) reverted to the pattern exhibited by bifunctional DAG (BFDAG) upon illumination. The diazirine moiety (green signals) is unaffected by uncaging and is only activated by UV light of >355 nm. Crucially, the alkyne group remained intact through all illumination steps (cyan signals in Fig. 1*D*), enabling subsequent functionalization.

Uncaging of Trifunctional Lipids in Living Cells. After establishing photochemical suitability, we applied trifunctional lipids to living cells to investigate their biocompatibility and signaling functionality. Intracellular Sph was reported to induce cytosolic calcium increase by release from acidic stores (1), whereas elevated DAG levels trigger rapid translocation of C1-domain-containing proteins to the plasma membrane (2). As expected, local uncaging of TFS led to Ca^{2+} transients for 40 to 80 s as measured by the cytosolic calcium dye Fluo-4. The kinetics of calcium release were comparable to previously demonstrated uncaging of native Sph (1). Importantly, the negative control compound dihydrosphingosine (dhSph) was unable to elicit calcium release under these conditions (Fig. 2 *A* and *B*). The effects of DAG elevation were monitored by the fluorescent biosensor C1-GFP. Adding the bifunctional DAG probe **10** to the medium of HeLa cells expressing C1-GFP led to translocation of the protein to the plasma membrane over the course of 2 min (Fig. 2*C*, *Upper*). Simple addition of TFDAG, on the other hand, failed to induce C1-GFP translocation, demonstrating its biological inertness in the caged form. Only 405-nm uncaging of TFDAG through the microscope objective induced translocation (Fig. 2*C*, *Lower*). It is important to note that illumination through the microscope objective only uncages a small fraction of the probe compared with biochemical bulk experiments that make use of strong UV lamps. The simultaneous uncaging of all probe molecules in such experiments can be used to investigate probe metabolism by TLC (Fig. S1). Here, cells labeled with 3 μM TFS or 50 μM TFDAG were subjected to pulse experiments; the resulting metabolites were visualized by click reaction (8) and separated on TLC. Unfortunately, the TFDAG probe partially fragmented during lipid extraction and click reaction thus preventing analysis by TLC (Fig. S1 *C* and *D*). TFS, on the other hand, was stable in cells (Fig. S1*A*) and was readily incorporated into sphingolipids as well as phospholipids upon uncaging (Fig. S1*B*), in accordance with previous studies using bifunctional sphingosine (20). Together with the results obtained by live-cell microscopy, this confirms that the diazirine and alkyne moieties do not impact on the biological activity of Sph and DAG, respectively, and that acute signaling events can be triggered by uncaging of trifunctional lipids.

Quantification of DAG Turnover at the Plasma Membrane. Being able to trigger C1-GFP translocation to the plasma membrane in a controlled fashion allowed us quantify lipid turnover on a population-wide as well as on a single-cell level, thereby accounting for the inherent heterogeneity of cell populations. Compared with standard biochemical experiments, such live-cell uncaging experiments also offer superior temporal resolution; however, they do not measure pure metabolism, as the signal acquired through biosensors accounts for both lipid transport and metabolic transformations.

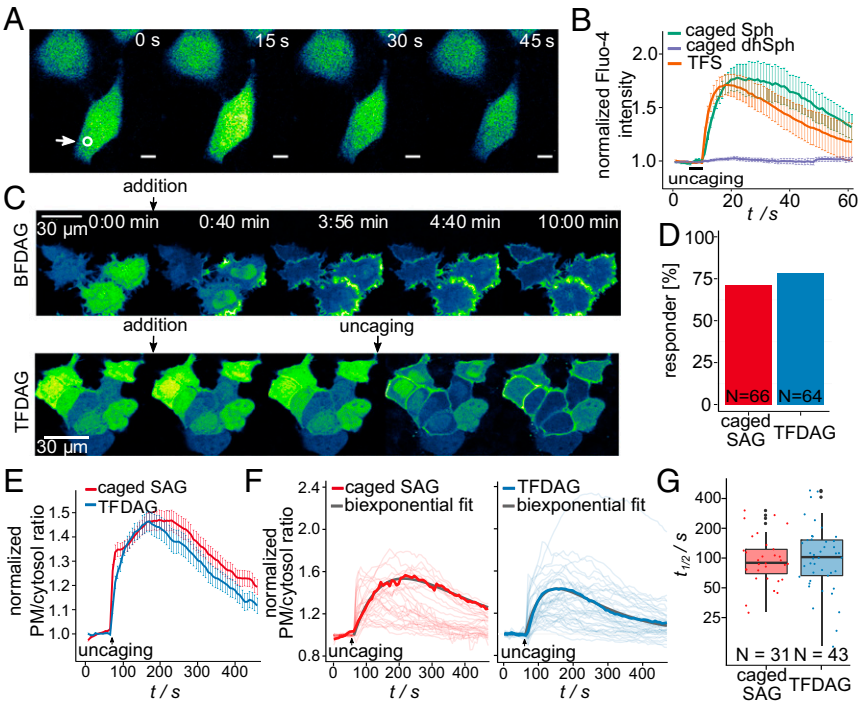

Fig. 2. Trifunctional lipids for the study of cellular signaling. (*A*) Time-lapse confocal microscopy images of HeLa cells labeled with Fluo-4 (a cytosolic calcium indicator) and 2 µM TFS **1**. Uncaging was performed by irradiation of a circular area within the cells (indicated by the white circle) for 3 s at t = 10 s. (*B*) Quantification of mean Fluo-4 fluorescence of cells loaded with 2 µM caged Sph, 2 µM caged dihydro-Sph, or 2 µM TFS. Traces represent mean values, with the SEM plotted as error bars. (*C*) Time-lapse montage of HeLa cells expressing C1-GFP and treated with 100 µM bifunctional SAG (BFDAG) **10** at t = 0:30 min (*Upper*) or treated with 100 µM TFDAG **2** at t = 0:30 min and uncaged by scanning the entire field of view with a 405-nm laser once at t = 4:00 min (*Lower*). (*D*) Response rates for C1-GFP translocation upon SAG and TFDAG uncaging. (*E*) Mean translocation traces for SAG and TFDAG uncaging with SEM plotted as error bars. (*F*) Individual traces after a quality control step with a representative trace and the corresponding biexponential fit highlighted. (*G*) Single-cell half-life times for DAG turnover for SAG and TFDAG.

Here, we performed a series of uncaging experiments using TFDAG and compared it to caged SAG (2) (Movies S1 and S2). Changes in plasma membrane DAG levels were quantified using the ratio between plasma membrane-bound and cytosolic fractions of C1-GFP as calculated using a recently developed algorithm (22) (see *SI Materials and Methods* for details). Most cells exhibited significant C1-GFP translocation to the plasma membrane, with similar response rates for TFDAG and SAG, respectively (TFDAG 78%, SAG 71%; Fig. 2*D*). Kinetic traces were measured for all cells (Fig. S2), and responding cells were included in the kinetic analyses. Mean translocation traces (Fig. 2*E*) showed an initial rapid increase of the C1-GFP plasma membrane/cytosol ratio, reflective of the rapid increase of DAG concentration caused by uncaging. After reaching a maximum ~100 s after illumination, the observed signal declined with comparable slopes for both lipids, indicating ongoing DAG turnover. To characterize their kinetics more quantitatively, we analyzed and fitted the responses on a single-cell level. A simple biexponential model featuring terms for C1-GFP recruitment to the plasma membrane and DAG turnover was fitted to the individual traces (see Fig. S3 and *SI Materials and Methods* for details). After quality control (SE estimate below 0.06 and a positive turnover rate; see *Supporting Information*), a set of 31 and 43 traces were obtained for SAG and TFDAG, respectively (Fig. 2*F*). The determined half-life times for DAG turnover (Fig. 2*G*) revealed striking differences on a cell-to-cell level, as individual cells exhibited DAG turnover rates varying over an order of magnitude. These data suggest that heterogeneity of signaling lipid turnover might be an underrated aspect in lipid signaling events.

Chemoproteomic Profiling of Lipid–Protein Complexes. A further application of trifunctional lipids is the systematic mapping of lipid–protein interactions by mass spectrometry. Owing to the two orthogonal photoreactions, which enable a "release and catch" approach, trifunctional lipids allow profiling the protein interactome of single lipid species. Due to the reduced complexity of the bait compared with bifunctional lipids, this screening technology is more sensitive to low-abundance lipids and should pick up scarce lipid–protein interactions. HeLa cells were labeled with 6 µM TFS and 100 µM TFDAG or TFFA, which resulted in comparable loading of the cells, owing to their different uptake kinetics (Fig. S4). After uncaging and photoaffinity labeling, the protein–lipid conjugates were reacted with biotin azide using copper-catalyzed click chemistry and subsequently enriched via neutravidin beads. The preparation of peptides for proteomic analysis was performed according to a recent protocol optimized for ultrasensitive analysis of complex biological samples (23). Using this method, a total of 3,263 proteins were identified. For further analysis, only proteins that were identified in both screens using either TFS or TFDAG were considered. The peptide spectral matches of these high-confidence proteins are displayed as a heat map in Fig. 3*A*. As noted in previous studies using bifunctional lipids (20, 21), a high overlap in the interactome of different lipids was observed; this may be attributed to unspecific cross-linking of highly abundant proteins with either probe or background binding to the beads during the pull-down procedure, highlighting the need for control lipids. By grouping the resulting proteins according to the ratio of their peptide spectral matches over control lipids, we were able to identify two subsets of proteins, which interacted preferentially with either TFS (Fig. 3*A*, top left group) or TFDAG (Fig. 3*A*, bottom right group); a sample 55 hits are displayed for TFS and TFDAG, respectively. The full list of proteins arranged as in Fig. 3*A* as well as lists for Sph- and DAG-interacting proteins can be found in Dataset S1. Reassuringly, we found proteins previously reported to interact with Sph [ceramide synthase 2, which uses Sph as a substrate (24), and cathepsin B, which is a mediator of Sph-induced apoptosis (25)] or with DAG [phosphatidylinositol 4,5-bisphosphate phosphodiesterase delta 3, a DAG producing enzyme (26)] among our top hits. We then compared the list of putative Sph-interacting proteins from this screen with results from a previous screen performed with bifunctional Sph (20) (Fig. S5*A*). Fourteen proteins were already detected using bifunctional Sph, further strengthening them as bona fide Sph binders. However, the majority of these proteins were not previously identified. Here, we benefited from the major advantage of trifunctional lipids to circumvent lipid metabolism and identify scarcer or very short-lived lipid–protein interactions. In the absence of previous proteomic screens with DAG as bait, we compared proteins identified using TFDAG to hits from previous screens performed with bifunctional endocannabinoid probes (21). These probes contain arachidonic acid just as TFDAG does. Reassuringly, only 17 of 130 putative DAG-interacting proteins were previously identified using the endocannabinoid probes (Fig. S5*B*), which further confirms

that proteins identified with TFDAG are specifically interacting with DAG.

Subcellular Localization of Lipids and Lipid-Interacting Proteins. To further analyze these new, putative Sph and DAG-interacting proteins, we accessed their gene ontology (GO) terms and compared the annotated subcellular localizations of TFS and TFDAG hits (Fig. 3*B*). A larger percentage of TFS interactors were annotated to the secretory pathway [endoplasmic reticulum (ER), Golgi, vesicles, endosomes, lysosomes, and exosomes] compared with TFDAG hits, which are mainly annotated as cytosolic proteins. This result hints toward a different subcellular localization of the trifunctional lipids at the time of cross-linking. Before uncaging, trifunctional lipids are indiscriminately localized to internal membranes and the cytoplasm as visualized by fluorescence of the coumarin caging group (Fig. S6*A*, *Upper*). To investigate their localization at the time of cross-linking, HeLa cells were treated in the same way as for the proteomic screens, but followed by fixing and staining of the lipid–protein complexes with Alexa488-azide (Fig. 3*C* and Fig. S6*A*, *Lower*). We observed that each lipid now localized to distinct cellular compartments. Strikingly, the staining of TFDAG resulted in 52 to 59% weaker fluorescence compared with TFS and TFFA, respectively (Fig. S6*B*). Cytosolic and nuclear proteins are known to be extracted by methanol fixation (27), which is necessary for this protocol, as it removes all non–cross-linked lipids. This may explain the reduced fluorescence intensity in these regions and confirms the GO-term analysis of DAG-interacting proteins, which listed surprisingly many cytosolic proteins. We speculate that the high proportion of cytosolic proteins likely reflects a highly efficient DAG transporting machinery, which requires extraction of DAG from membranes, thereby potentially exposing the cross-linkable group. For example, extended synaptotagmins (E-Syts) were recently shown to extract DAG from the plasma membrane (28). Accordingly, we identified both E-Syt1 and E-Syt2 in screens performed with TFDAG. However, E-Syt1 was also found using TFS and TFFA, and E-Syt2 was identified with TFS but not with TFFA, hinting at a broader lipid specificity of these proteins. TFS, on the other hand, was found to be predominantly localized to the perinuclear ER, Golgi, and, mainly, endosomes/lysosomes (see Fig. S6 *C*, *E*, and *F* for colocalization). We quantified the amount of Sph labeling in LAMP1-stained compartments to 40% of total fluorescence, whereas the more uniform labeling of TFDAG only localized 22% of total fluorescence to areas also marked by LAMP1 (Fig. S6*D*).

Sphingosine Localization in Niemann–Pick Disease Type C. To highlight the potential of trifunctional lipids for the visualization of subcellular lipid localization, we chose as an example the study of Niemann–Pick disease type C (NPC) cells. NPC is a rare lysosomal storage disease caused mainly by mutation of the gene encoding for the NPC1 protein (29). In diseased cells, Sph is known to accumulate alongside other lipids such as sphingomyelin, cholesterol, and higher glycosphingolipids (30, 31). The function of NPC1 is not fully understood, but NPC cells exhibit a trafficking defect at the late endosomal/lysosomal stage, as observed for cholesterol by using Filipin staining (32). Accumulation of Sph and lactosylceramide was previously visualized using fluorescent lipid analogs (33, 34). Here, we used TFS to visualize Sph localization and trafficking. To create a cellular model of NPC, HeLa cells were either treated with the cationic amphiphilic drug U18666A, which acts as an NPC1 inhibitor (35), or with siRNA targeted to NPC1. Both treatments produced an NPC phenotype, as confirmed by Filipin staining (Fig. S7*A*). Using TFS on these cell models, a noticeable increase of fluorescence was observed in late endosomal/lysosomal vesicles (Fig. 4*A*; for colocalization, see Fig. S7*B*), indicative of Sph storage.

Sphingosine Transport in NPC. We then investigated whether the transport of Sph out of the acidic compartment was affected as well. Here, the main advantages of trifunctional lipids became

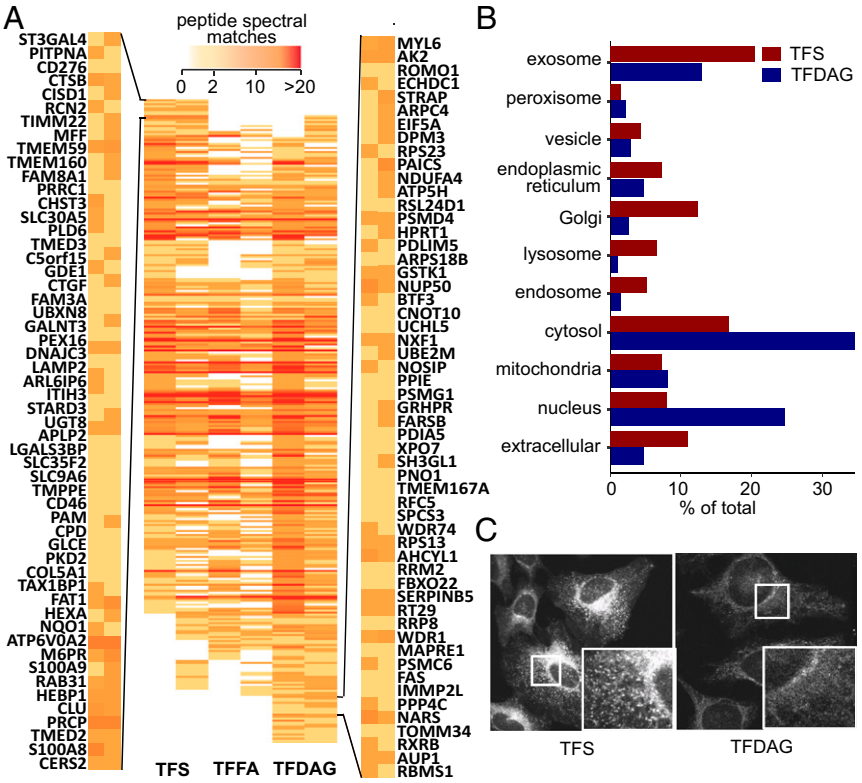

Fig. 3. Mass spectrometric identification of Sph- and SAG-binding proteins. (*A*) Heat map of high-confidence proteins identified in both screens. Peptide spectral matches are color-coded according to the legend on the top. Proteins are arranged such that preferential TFS interactors are displayed on the top (the gene symbols for the first 55 proteins are displayed on the left) and TFDAG interactor are grouped near the bottom (55 proteins are displayed on the right). (*B*) Putative Sph- and DAG-binding were analyzed according to their cellular compartment (CC) GO terms. (*C*) Confocal microscopy images of HeLa cells labeled with TFS (*Left*) and TFDAG (*Right*) under the conditions used in the proteomic experiments. Cells were fixed with methanol, non–cross-linked lipids were washed away, and the remaining cross-linked lipids were clicked to Alexa488-azide.

obvious: By using two photoreactions (uncaging/cross-linking), it was possible to bypass the uptake and possible retention of Sph in the endocytic pathway and to set up pulse–chase experiments. The accumulation of bifunctional Sph **4** in acidic compartments after uncaging set a precise starting point for quantifying transport of Sph and its metabolites out of the acidic compartment. In control cells, Sph was rapidly (<10 min) cleared from the vesicles, as exemplified by a drop in Pearson's correlation coefficient with the late endosomal/lysosomal marker LAMP1 (Fig. S7*B*). Both NPC models (U18666A and siRNA), on the other hand, retained most Sph in the late endosomal/lysosomal vesicles even after 30-min postuncaging (Fig. 4*A*), as expected for cells with lipid transport defect. Next, we investigated Sph transport in skin fibroblasts derived from three NPC patients with varying disease severity. Cells derived from the patient with the mildest phenotype were able to export most of the lysosomal Sph within 10 min, whereas the more severe patients still showed marked lysosomal Sph accumulation after 30 min (Fig. 4*B*). We quantified this retention by investigating the skewness of the pixel distribution in each cell through automated image processing (Fig. 4*C*). High skewness values represent vesicular staining, whereas lower values are indicative of an even distribution throughout the cells as achieved by ER or internal membrane staining.

Ultrastructural Localization of Sphingosine. To further examine this accumulation on an ultrastructural level, we subjected NPC patient fibroblasts to high-precision CLEM. Briefly, cross-linked lipids were functionalized with Alexa594-azide followed by high-pressure freezing (HPF) and thin sectioning. Fluorescent and electron dense fiducial marker beads (36) were used to correlate fluorescence images and electron tomograms (Fig. 4*D*). We found that Sph localized to intraluminal vesicles of late endosomes/multivesicular bodies, which strengthens the hypothesis of a trafficking block at the late endosomal stage.

Discussion

We have developed a photochemical probe type featuring two sequential photoreactions, which allows different aspects of lipid biology to be studied while using the same molecule. Importantly, trifunctional lipids constitute a unique way to investigate single lipid species in a live-cell setting, which is especially important when looking at active signaling lipid species. We successfully used these probes to quantify cellular signaling after uncaging by live-cell imaging of downstream effects including C1-domain translocation and changes of calcium levels. Trifunctional lipids have furthermore proven useful in the unbiased identification of novel, putative Sph and DAG-interacting proteins by proteomic analysis. Some of the identified, high-confidence interactors open up exciting avenues for further study: For example, we found beta-hexosaminidase A and B (HexA and HexB) to interact with Sph. It is interesting to speculate that Sph might act as regulator of lipid-catabolizing enzymes such as HexA, the activity of which is known to depend on the lipid composition of the substrate membranes (37). Such a potential regulation of HexA by Sph might thereby further contribute to lipid storage diseases such as NPC, which accumulate glycosphingolipids. A further application of trifunctional lipids lies in the visualization of their subcellular localization by fluorescence microscopy and CLEM. Reassuringly, the annotated cellular compartments of the identified proteins corresponded well with their observed localization. Taking this further, we set up an assay to investigate the transport of Sph in NPC disease and observed a trafficking block at the late endosomal stage. For the future, we imagine that this

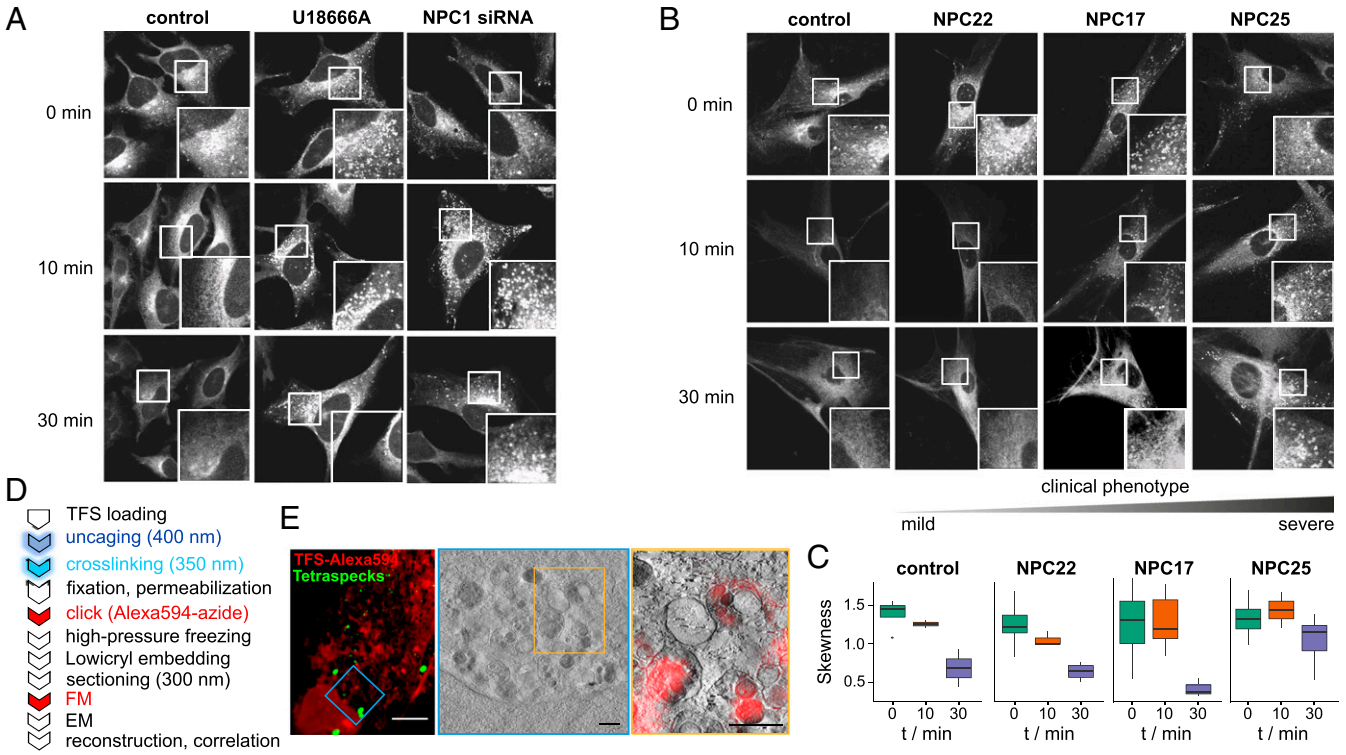

Fig. 4. Sph localization and transport in NPC models. (*A*) Confocal images of Sph stained with Alexa488-azide in HeLa cells in control conditions or upon induction of the NPC cellular phenotype by U18666A (2 μg/mL for 24 h) or by siRNA-mediated knockdown of NPC1. Pulse–chase experiments were performed by varying the time between uncaging and cross-linking from 0 min to 30 min. (*B*) Confocal images of Sph stained with Alexa488-azide in human fibroblasts derived from a healthy donor (control) or from NPC patients with varying genotypes and severity scores (NPC22, NPC17, NPC25). Pulse–chase experiments were performed as in *A*. (*C*) Quantification of human fibroblasts by automated image analysis. Skewness values for each cell were extracted and plotted according to cell line and time after uncaging. (*D*) Workflow for CLEM of NPC fibroblasts. EM, electron microscopy; FM, fluorescence microscopy. (*E*) CLEM images of NPC fibroblast labeled with TFS according to the procedure in *D*.

trafficking assay could serve as a valuable diagnostic tool complementing the established Filipin staining analysis, as it is independent of cholesterol accumulation but assays the capability of the cells to move Sph out of late endosomes/lysosomes. In the three NPC cell lines investigated, the observed Sph transport correlated well with patients' severity scores. However, further tests on a larger number of patient samples will be necessary to confirm that Sph retention in the late endosomes/lysosomes is a marker for disease severity.

In conclusion, we demonstrated the practicality of trifunctional lipids for studying different aspects of lipid biology in the context of living cells, and we envision that this design will lead to the generation of more trifunctional lipids and studies of the relevant signaling networks.

Materials and Methods

Chemical Synthesis and Cell Culture. Detailed protocols for the synthesis of trifunctional lipids and their characterization data (Dataset S2) as well as information about cell lines and their culture conditions can be found in *SI Materials and Methods*.

Confocal Uncaging Experiments. HeLa cells were transfected with C1-GFP 24 h before experiments. For calcium imaging, cells were labeled with 100 μL of 5 μM Fluo-4 AM for 30 min before the experiment. Cells were treated with a 100 μM solution of TFDAG/caged SAG or a 2 μM solution of TFS in imaging buffer. Confocal time lapses were acquired at 37 °C, and uncaging was performed by either scanning the entire field of view with a 405-nm laser or by spot-uncaging for 3 s at 2 μs per pixel. For more detailed protocols, please refer to *SI Materials and Methods*.

Lipid Analysis by TLC. Briefly, cells were labeled with 3 μM TFS or 50 μM TFDAG for the indicated times and subjected to UV-induced uncaging, as indicated. Cellular lipids were extracted, labeled with 3-azido-7-hydroxycoumarin via click reaction, separated on a TLC plate, and visualized via the coumarin fluorescence.

Proteomic Screens. A detailed procedure can be found in *SI Materials and Methods*. Briefly, HeLa cells were labeled with trifunctional lipids and UV-irradiated for 2.5 min at >400 nm and for another 2.5 min >345 nm. The lysate was subjected to click reaction with biotin azide, and protein–lipid complexes were enriched using NeutrAvidin. Proteins were digested according to a recently developed protocol (23) and subjected to high-pH fractionation (38). Peptides were separated using the nanoAcquity ultra performance liquid chromatography (UPLC) system coupled directly to a linear trap quadrupole (LTQ) OrbitrapVelos Pro using the Proxeon nanospray source.

Visualization of Lipid–Protein Complexes. A detailed protocol for visualizing lipid localization in cells by fluorescent microscopy as well as by correlated light and electron microscopy can be found in *SI Materials and Methods*.

ACKNOWLEDGMENTS. We thank the Advanced Light Microscopy Facility and the Proteomic Core Facility of the European Molecular Biology Laboratory (EMBL). This research has received funding from the European Union Seventh Framework Programme under Grant Agreement 289278—"Sphingonet"—as well as Transregio 83 funded by the Deutsche Forschungsgemeinschaft. This work was partially supported by the intramural research program of the National Institute of Child Health and Human Development. M.S. is a fellow of the EMBL Interdisciplinary Postdoc Program, cofunded by the European Union.

1. Höglinger D, et al. (2015) Intracellular sphingosine releases calcium from lysosomes. *eLife* 4:e10616.
2. Nadler A, et al. (2013) The fatty acid composition of diacylglycerols determines local signaling patterns. *Angew Chem Int Ed Engl* 52(24):6330–6334.
3. Feng S, et al. (2014) A rapidly reversible chemical dimerizer system to study lipid signaling in living cells. *Angew Chem Int Ed Engl* 53(26):6720–6723.
4. Idevall-Hagren O, Dickson EJ, Hille B, Toomre DK, De Camilli P (2012) Optogenetic control of phosphoinositide metabolism. *Proc Natl Acad Sci USA* 109(35):E2316–E2323.
5. Höglinger D, Nadler A, Schultz C (2014) Caged lipids as tools for investigating cellular signaling. *Biochim Biophys Acta* 1841(8):1085–96.
6. Mentel M, Laketa V, Subramanian D, Gillandt H, Schultz C (2011) Photoactivatable and cell-membrane-permeable phosphatidylinositol 3,4,5-trisphosphate. *Angew Chem Int Ed Engl* 50(16):3811–3814.
7. Hövelmann F, et al. (2016) Optotaxis: Caged lysophosphatidic acid enables optical control of a chemotactic gradient. *Cell Chem Biol* 23(5):629–634.
8. Thiele C, et al. (2012) Tracing fatty acid metabolism by click chemistry. *ACS Chem Biol* 7(12):2004–2011.
9. Matyas GR, Beck Z, Karasavvas N, Alving CR (2009) Lipid binding properties of 4E10, 2F5, and WR304 monoclonal antibodies that neutralize HIV-1. *Biochim Biophys Acta* 1788(3):660–65.
10. Alvarez-Vasquez F, et al. (2005) Simulation and validation of modelled sphingolipid metabolism in *Saccharomyces cerevisiae*. *Nature* 433(7024):425–430.
11. Kuerschner L, et al. (2005) Polyene-lipids: A new tool to image lipids. *Nat Methods* 2(1):39–45.
12. Nishioka T, et al. (2008) Rapid turnover rate of phosphoinositides at the front of migrating MDCK cells. *Mol Biol Cell* 19(10):4213–4223.
13. Manifava M, et al. (2001) Differential binding of traffic-related proteins to phosphatidic acid- or phosphatidylinositol (4,5)- bisphosphate-coupled affinity reagents. *J Biol Chem* 276(12):8987–8994.
14. Gallego O, et al. (2010) A systematic screen for protein–lipid interactions in *Saccharomyces cerevisiae*. *Mol Syst Biol* 6(1):430.
15. Saliba A-E, et al. (2014) A quantitative liposome microarray to systematically characterize protein-lipid interactions. *Nat Methods* 11(1):47–50.
16. Ceccato L, et al. (2016) PLIF: A rapid, accurate method to detect and quantitatively assess protein-lipid interactions. *Sci Signal* 9(421):rs2.
17. Haberkant P, Holthuis JCM (2014) Fat & fabulous: Bifunctional lipids in the spotlight. *Biochim Biophys Acta* 1841(8):1022–1030.
18. Haberkant P, et al. (2013) In vivo profiling and visualization of cellular protein-lipid interactions using bifunctional fatty acids. *Angew Chem Int Ed Engl* 52(14):4033–4038.
19. Hulce JJ, Cognetta AB, Niphakis MJ, Tully SE, Cravatt BF (2013) Proteome-wide mapping of cholesterol-interacting proteins in mammalian cells. *Nat Methods* 10(3):259–264.
20. Haberkant P, et al. (2016) Bifunctional sphingosine for cell-based analysis of protein-sphingolipid interactions. *ACS Chem Biol* 11(1):222–230.
21. Niphakis MJ, et al. (2015) A global map of lipid-binding proteins and their ligandability in cells. *Cell* 161(7):1668–1680.
22. Nadler A, et al. (2015) Exclusive photorelease of signalling lipids at the plasma membrane. *Nat Commun* 6:10056.
23. Hughes CS, et al. (2014) Ultrasensitive proteome analysis using paramagnetic bead technology. *Mol Syst Biol* 10(757):757.
24. Levy M, Futerman AH (2010) Mammalian ceramide synthases. *IUBMB Life* 62(5):347–356.
25. Kågedal K, Zhao M, Svensson I, Brunk UT (2001) Sphingosine-induced apoptosis is dependent on lysosomal proteases. *Biochem J* 359(Pt 2):335–343.
26. Pawelczyk T, Matecki A (1999) Phospholipase C-delta3 binds with high specificity to phosphatidylinositol 4,5-bisphosphate and phosphatidic acid in bilayer membranes. *Eur J Biochem* 262(2):291–298.
27. Hoetelmans RW, et al. (2001) Effects of acetone, methanol, or paraformaldehyde on cellular structure, visualized by reflection contrast microscopy and transmission and scanning electron microscopy. *Appl Immunohistochem Mol Morphol* 9(4):346–351.
28. Saheki Y, et al. (2016) Control of plasma membrane lipid homeostasis by the extended synaptotagmins. *Nat Cell Biol* 18(5):504–515.
29. Vanier MT (2010) Niemann–Pick disease type C. *Orphanet J Rare Dis* 5:16.
30. te Vruchte D, et al. (2004) Accumulation of glycosphingolipids in Niemann-Pick C disease disrupts endosomal transport. *J Biol Chem* 279(25):26167–26175.
31. Lloyd-Evans E, et al. (2008) Niemann-Pick disease type C1 is a sphingosine storage disease that causes deregulation of lysosomal calcium. *Nat Med* 14(11):1247–1255.
32. Sokol J, et al. (1988) Type C Niemann-Pick disease. Lysosomal accumulation and defective intracellular mobilization of low density lipoprotein cholesterol. *J Biol Chem* 263(7):3411–3417.
33. Sun X, et al. (2001) Niemann-Pick C variant detection by altered sphingolipid trafficking and correlation with mutations within a specific domain of NPC1. *Am J Hum Genet* 68(6):1361–72.
34. Blom T, Li Z, Bittman R, Somerharju P, Ikonen E (2012) Tracking sphingosine metabolism and transport in sphingolipidoses: NPC1 deficiency as a test case. *Traffic* 13(9):1234–1243.
35. Lu F, et al. (2015) Identification of NPC1 as the target of U18666A, an inhibitor of lysosomal cholesterol export and Ebola infection. *eLife* 4:1–16.
36. Kukulski W, et al. (2011) Correlated fluorescence and 3D electron microscopy with high sensitivity and spatial precision. *J Cell Biol* 192(1):111–119.
37. Sandhoff K (2016) Neuronal sphingolipidoses: Membrane lipids and sphingolipid activator proteins regulate lysosomal sphingolipid catabolism. *Biochimie* 130:146–151.
38. Bock T, et al. (2014) An integrated approach for genome annotation of the eukaryotic thermophile Chaetomium thermophilum. *Nucleic Acids Res* 42(22):13525–13533.
39. Shimada Y, Usuda K, Okabe H, Suzuki T, Matsumoto K (2009) Deracemization of 1,2-diol monotosylate derivatives by a combination of enzymatic hydrolysis with the Mitsunobu inversion using polymer-bound triphenylphosphine. *Tetrahedron Asymmetry* 20(24):2802–2808.
40. Sato S, et al. (2012) Occurrence of a bacterial membrane microdomain at the cell division site enriched in phospholipids with polyunsaturated hydrocarbon chains. *J Biol Chem* 287(29):24113–24121.
41. Stein F, Kress M, Reither S, Piljić A, Schultz C (2013) FluoQ: A tool for rapid analysis of multiparameter fluorescence imaging data applied to oscillatory events. *ACS Chem Biol* 8(9):1862–1868.
42. Wickham H (2009) ggplot2: Elegant Graphics for Data Analysis (Springer, New York).
43. Smedley D, et al. (2015) The BioMart community portal: An innovative alternative to large, centralized data repositories. *Nucleic Acids Res* 43(W1):W589–W598.
44. Avinoam O, Schorb M, Beese CJ, Briggs JAG, Kaksonen M (2015) Endocytic sites mature by continuous bending and remodeling of the clathrin coat. *Science* 348(6241):1369–1372.
45. Kukulski W, et al. (2012) Precise, correlated fluorescence microscopy and electron tomography of lowicryl sections using fluorescent fiducial markers. *Methods Cell Biol* 111:235–257.
46. Kremer JR, Mastronarde DN, McIntosh JR (1996) Computer visualization of three-dimensional image data using IMOD. *J Struct Biol* 116(1):71–76.